Two-Dimensional Radar Backscattering Modeling of Oil Slicks at Sea Based on the Model of Local Balance: Validation of Two Asymptotic Techniques for Thick Films

Nicolas Pinel, *Member, IEEE*, Christophe Bourlier, *Associate Member, IEEE*, and Irina Sergievskaya

***Abstract*—The problem of hydrodynamic modeling of the surfaces of oil films at sea is treated by using physical models, namely, the model of local balance and the Elfouhaily *et al.* spectrum model for describing the clean sea surface. Then, this refined hydrodynamic modeling of the surfaces of contaminated seas makes it possible to derive electromagnetic modeling by considering thin oil films on the sea surface. Two simplifying approaches in dealing with this complex double-layer problem are described, called "thin-layer" and "classical" approaches. These two approaches, both having the advantage of reducing to a single-layer problem, are compared with a rigorous reference method for 2-D problems. Thus, their validity domains are analyzed in terms of incidence angle, wind speed, polarization, frequency, and oil viscosity. Finally, the polarimetric behavior of both clean and contaminated seas is analyzed; following recent work led on satellite measurements, the same features are retrieved, and the influence of incidence angle, frequency, and oil viscosity can be studied.**

***Index Terms*—Hydrodynamics, oil slicks, sea surface electromagnetic scattering, thin films, water pollution.**

I. Introduction

THE problem of remote sensing of oil spills on sea surfaces is a challenging topic of investigation, which has been subject to active research over the last decades [1] and remains an active topic of investigation [2]–[24]. Most of the literature on this topic deals with analysis of data [14], particularly by SAR [5], [7], [8], [12], [15], [17], [24]. Then, only a few recent works (e.g., [2]–[4], [9]–[11], [19], [20], [25], and [26]) deal with quantitative electromagnetic modeling of sea oil spills.

Manuscript received October 23, 2012; revised February 14, 2013; accepted April 8, 2013. Date of publication July 11, 2013; date of current version March 3, 2014. This work was supported by The French National Research Agency (ANR) as part of the 2009 Ecotech programme through the project called "POLHSAR," which aimed at intensifying radar monitoring to combat deliberate marine pollution more effectively. The other involved partners were Thales Systèmes Aéroportés and CLS. It has also been supported by the Program RAS Radiophysics and Support of the Russian Government under Grants 11.G34.31.0048 and 11.G34.31.0078.

N. Pinel and C. Bourlier are with the Institut d'Électronique et de Télécommunications de Rennes (IETR) Laboratory (UMR CNRS 6164), LUNAM University of Nantes, 44306 Nantes Cedex 3, France (e-mail: nicolas.pinel@gmail.com; christophe.bourlier@univ-nantes.fr).

I. Sergievskaya is with the Institute of Applied Physics, Russian Academy of Sciences, 603600 Nizhny Novgorod, Russia (e-mail: i.sergia@hydro.appl.sci-nnov.ru).

Color versions of one or more of the figures in this paper are available online at http://ieeexplore.ieee.org.

Digital Object Identifier 10.1109/TGRS.2013.2259498

Contrary to other papers dealing with water-in-oil emulsions [2], [3] which occur for moderate to high wind conditions, this paper focuses on homogeneous insoluble oil films on the sea surface, which restricts our study to low to moderate wind conditions ($u_{10} \lesssim 8-10$ m/s) [11], [12], [27]. Moreover, in order to better understand and to thoroughly analyze the observed data, it is necessary to develop models of electromagnetic wave scattering by clean and contaminated seas. This implies, first, an appropriate hydrodynamic modeling to be able to correctly qualify and quantify the electromagnetic scattering phenomena. In this paper, contrary to other hydrodynamic models of surface damping due to surface films [28], [29] used in the literature which are not well adapted to oil slicks, a physical model well adapted to oil slick surface damping [30] is used, namely, the model of local balance (MLB).

Then, the electromagnetic modeling is derived. In this paper, similar to previous work [11] (which considered the Marangoni damping coefficient [28] for hydrodynamic oil damping), a "thin-layer" (TL) asymptotic approach is used. The classical approach which assumes that the electromagnetic wave cannot see the oil layer [4], [26] is also used and compared. For a 2-D problem, a very good agreement was found in [11] between asymptotic models using the TL approach and the numerical reference method for radar frequencies, for frequency $f = 3$ GHz, wind speed $u_{10} = 10$ m/s, and incidence angle $\theta_i = \{0; 20\}^\circ$, by considering the Marangoni damping with two film thicknesses $H = \{1, 10\}$ mm. Here, by using the MLB for the oil film surfaces, the validity domain of the TL approximation is studied for a 2-D problem more thoroughly and more generally: We study it directly on the numerical reference method with respect to the simulation parameters f, u_{10}, and θ_i, focusing on the monostatic configuration. The same way is used for the classical approach.

Finally, a polarimetric study is led by analyzing the polarization ratio with respect to the observation angle, for varying the frequency and the oil viscosity. Former observations made on satellite measurements [12], [18] are retrieved.

This paper is organized as follows. Section II presents the hydrodynamic modeling of both clean and contaminated seas by studying their surface spectra for two wind speeds and different oil film thicknesses and oil viscosities. Then, Section III presents the consecutive electromagnetic modeling for 2-D problems, in order to validate the TL and "classical"

approaches. These two simplifying approaches are first presented in Section III-A, and their validity domain is analyzed in detail in Section III-B with respect to the observation angles, for varying configurations. Finally, Section III-C analyzes the polarimetric behavior of contaminated seas by comparison with clean seas.

II. Hydrodynamic Modeling: MLB

In order to correctly predict the mechanisms of electromagnetic scattering from sea-like surfaces, beforehand, an appropriate hydrodynamic modeling of concerned rough surfaces is necessary. First, for both clean and contaminated seas, the surfaces are assumed to obey Gaussian height probability density function (pdf). Second, an appropriate model for describing the surface height spectrum is needed. In this paper, for the case of clean seas, the Elfouhaily *et al.* surface height spectrum model [31] is considered. This is a widely used model which very satisfactorily simulates the sea surface behavior for fully developed seas and for low to moderate wind speeds at microwave frequencies. For the case of contaminated seas, the Elfouhaily *et al.* model is also used, in conjunction with a model which simulates the damping of the surface heights due to the presence of the oil film. It is assumed that the two (air/oil and oil/sea) interfaces of the contaminated sea obey the same statistics, i.e., have the same surface height pdf and spectrum.[1] Here, the study focuses on homogeneous insoluble oil films, which restricts our study to low to moderate wind speeds, i.e., $u_{10} \lesssim 8{-}10$ m/s [11], [12], [27].

A. MLB

In the literature, to our knowledge, only a few models that predict the hydrodynamic damping of rough surfaces in the presence of surface films and that can deal with oil films can be found [28]–[30]. The first model [28] can be applied to oil films only for monomolecular films, and the second model can be applied [29] only for thin oil films with thickness H, checking the condition $H \ll \sqrt{\nu/\omega}$, with ν as the volume viscosity and ω as the wave pulsation (for more details, see [19]). Thus, the third one [30] is the most appropriate, in general, for our study.

Being called the MLB, this is a physical and refined damping model which takes account of the impact of oil films on the wind waves [19], [30]. It is worth noticing that numerous field experiments demonstrated that the damping due to the oil film does not depend on the wind direction [30]; then, this model was built to check this property. This model is detailed in [30], and the damping ratio (the ratio between the spectra of clean and contaminated sea surfaces) is given by the following expression [19]:

$$y_{s,\mathrm{MLB}}(k) = \left[\frac{\beta(u^*,k)-\gamma_{cl}(k)}{\beta(u^*,k)-\gamma_{ct}(k;H,PP)}\right]^n \text{ with } \times \begin{cases} n=+1 & \text{if } \beta>\gamma \\ n=-1 & \text{if } \beta<\gamma \end{cases} \quad (1)$$

[1]For thin oil films, further in the paper, the two surfaces will be considered as identical and parallel.

where $\beta(u^*,k)$ is the wind growth rate [32], with u^* as the friction velocity, which depends on the wind velocity u_{10}; $\gamma_{cl}(k) = 2\nu k^2$ is the wave viscous damping on the clean surface (with ν as the kinematic viscosity of water); and $\gamma_{ct}(k;H,PP)$ is the wave viscous damping on the contaminated surface, covered by an oil film of thickness H and with physical parameters denoted as PP. For monomolecular films ($H=0$), wave viscous damping depends only on the rheological parameters E_0 and ω_D of the oil film. In this case, the wave viscous damping is connected with the viscous damping coefficient given in the Lombardini *et al.* damping model. In the general case ($H \neq 0$), the wave viscous damping γ_{ct} depends on the film thickness H and on physical parameters PP: oil volume viscosity ν_{oil}; surface (air/oil) and interface (oil/water) tensions σ_+ and σ_-, respectively; surface and interface elasticities E_+ and E_-, respectively; and viscosities μ_+ and μ_-, respectively. These parameters were retrieved from the data of our laboratory experiment. Our analysis of wave damping showed that, for oil films of thicknesses on the order of millimeter (or thicker), the wave damping depends on oil viscosity but does not significantly vary with the elasticity of the oil/water boundary. Then, in this paper, we considered that the elasticity is fixed and studied the influence of the oil viscosity. Then, the MLB depends on two main physical parameters of the oil film: the film thickness H and the oil volume viscosity ν_{oil}. Recently, Fuks and Zavorotny [9] have proposed a practical damping model which cuts off the clean sea surface spectrum at a surface wavenumber k_c on the order of a few radians per meter. Nevertheless, a more precise value of k_c and its variation with respect to the oil film parameters must be determined.

First, the slope spectrum $k^2S(k)$ of the surfaces of clean and contaminated seas is plotted for two wind speeds and for oil films with two different viscosities and film thicknesses by using the MLB [30]. The curvature spectrum $k^3S(k)$ is also plotted for comparison as the classical electromagnetic model called small perturbation method (SPM) is directly proportional to $k_B^3S(k_B)$, with $k_B = 2k_0\sin\theta$ (with k_0 as the electromagnetic wavenumber and θ as the observation angle with respect to zenith), for a monostatic configuration. An illustration of corresponding generated surface slopes is given. Then, the rms slopes of the surfaces of clean and contaminated seas are plotted for wind speeds u_{10} ranging 2–10 m/s.

B. Surface Spectrum and RMS Slope

In Fig. 1, the isotropic parts of the *slope* spectrum $k^2S(k)$ of clean and contaminated sea surfaces $k^2S_{\mathrm{clean,iso}}(k) = k^2M(k)$ and $k^2S_{\mathrm{cont,iso}}(k) = k^2M(k)/y_s(k)$ [with y_s as the damping ratio given for the MLB by (1)], respectively, are plotted versus the surface wavenumber k. For a contaminated sea, the MLB [30] is applied for two different oil types and thicknesses. The oil type is either a heavy oil with viscosity $\nu_{\mathrm{oil}} = 0.5$ cm^2/s or a light oil with viscosity $\nu_{\mathrm{oil}} = 0.1$ cm^2/s, and the film thickness is either $H = 10$ μm or $H = 100$ μm. The wind speed is $u_{10} = 4$ m/s.

As expected, it can be seen that the oil film significantly damps the high frequencies, which corresponds to the capillary waves of the surface; the lower frequencies are nearly

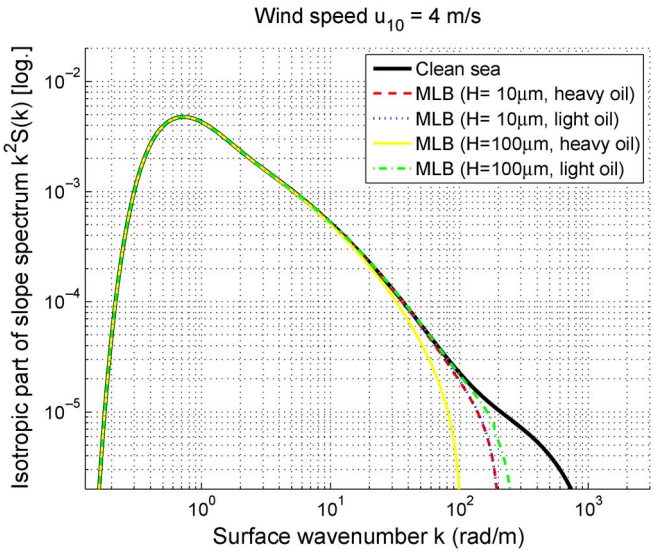

Fig. 1. Isotropic parts of the slope spectrum of clean and contaminated sea surfaces versus the surface wavenumber k (in radians per meter). For the contaminated sea, the MLB is applied for two different oil film types and thicknesses: with either heavy or light oils, having a film thickness $H = 10$ μm or $H = 100$ μm. The wind speed is $u_{10} = 4$ m/s.

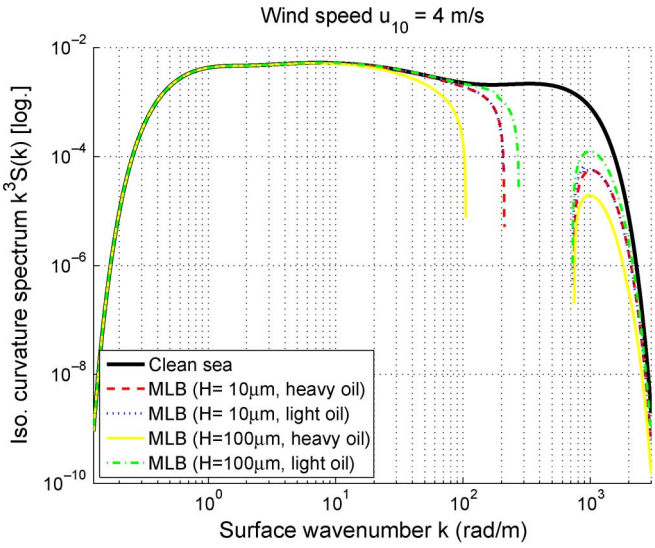

Fig. 2. Isotropic parts of curvature spectrum $k^3S(k)$ of clean and contaminated sea surfaces versus the surface wavenumber k, with the same parameters as in Fig. 1.

unaffected. Moreover, for the thinner film $H = 10$ μm, no significant difference between heavy and light oils is observed. On the contrary, for $H = 100$ μm, significant differences appear: The damping is stronger and begins to contribute at lower surface wavenumbers for the heavier oil. Finally, interestingly, for the heavy oil, as expected, the damping is stronger for $H = 100$ μm than for $H = 10$ μm, but it is the opposite for the light oil. As a consequence, more thorough analysis was led (not shown here) to study the damping behavior with respect to the thickness, for $H = \{0; 10; 50; 100; 500; 1000\}$ μm. First, for the heavy oil with $\nu_{\text{oil}} = 0.5$ cm^2/s, for $H = \{0; 10; 50\}$ μm, and for small thicknesses ($H = \{0; 10; 50\}$ μm), the damping does not vary significantly when H increases, whereas for greater thicknesses ($H = \{50; 100; 500; 1000\}$ μm), the damping significantly becomes greater when H increases. Second, for the light oil with $\nu_{\text{oil}} = 0.1$ cm^2/s, the damping slightly increases for increasing H.

We can highlight here the relevance of the simple damping model used by Fuks and Zavorotny [9], which considers a cutting off in the surface spectrum. More precisely, three values of the surface wavenumber are tested: $k_c = 2\pi/L_c = \{6.3; 10.5; 20.9\}$ rad/m. Nevertheless, several limitations of this model can be highlighted. Among others, the value of this cutting off seems to be chosen empirically and does not depend either on physical parameters like the oil viscosity and film thickness or on the wind speed. Moreover, in the case plotted in Fig. 1, these values seem to be a bit too low. Also, even if the damping appears as very strong in decibel scale, approximating it by a cutoff remains an approximation which would deserve to be analyzed and validated.

For sea-like surfaces at monostatic configuration and small to moderate winds, for angles $\theta \gtrsim 40°$, the scattering process is mainly governed by SPM which writes that the normalized radar cross section (NRCS) is proportional to $k_B^3 S(k_B)$ for 2-D problems and to $k_B^4 S(k_B)$ for 3-D problems (by contrast, for

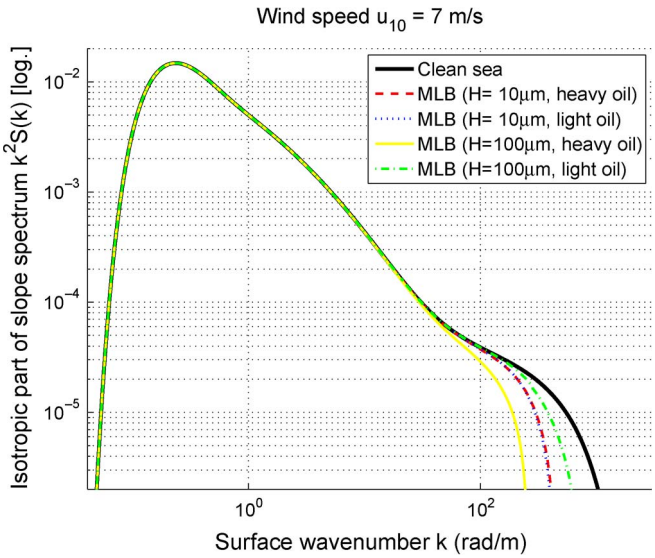

Fig. 3. Simulations for the same parameters as in Fig. 1, except for the wind speed $u_{10} = 7$ m/s.

angles $0° \leq \theta \lesssim 20°$, it is mainly governed by geometric optics (GO) approximation which is related to the surface rms slope). Then, let us have a look at the curvature spectrum $k^3S(k)$ for clean and contaminated seas. It is plotted in Fig. 2 for the same parameters as previously. Compared to the slope spectrum, it can be seen that the curvature spectrum significantly increases the higher frequencies of the spectrum; that is why a refined description of the capillary waves is essential for correctly predicting the radar backscattering NRCS when SPM dominates the scattering process. This feature is of interest as, even if SPM is not sufficient to explain the polarimetric behavior of the backscattering, for thin oil films, it was shown to provide good indications about the damping ratio (clean/polluted radar return ratio) of a single polarimetric channel [33].

In order to study the influence of wind speed on the damping, Fig. 3 plots the slope spectrum for the same parameters as in

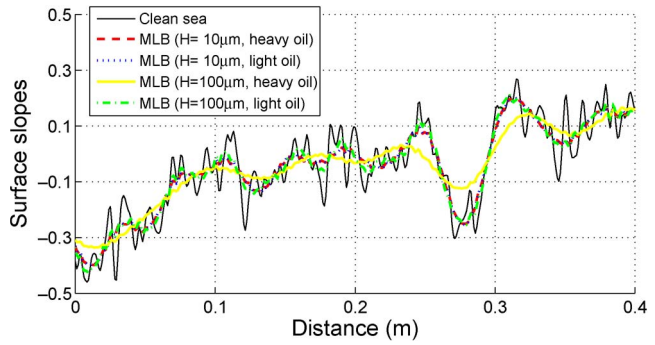

Fig. 4. Representation of the slopes of a particular generated sea surface, for clean and contaminated seas, with the same parameters as in Fig. 1.

Fig. 1, except for a higher wind speed: $u_{10} = 7$ m/s. It can be seen that increasing the wind speed induces an increase of the surface wavenumber limit over which a significant damping occurs. As a consequence, the differences between clean and contaminated seas decrease, as illustrated further in the rms slope. Note that this observation is in agreement with measurement observations which conclude that the most accepted upper limit of detection is about 10 m/s [21].

In what follows, the impact of the oil damping on the surface slopes is studied. Let us note that, contrary to the surface *slopes*, for the surface *heights*, no difference between the clean and contaminated cases is observed. This implies that the oil damping has no significant observable impact on the surface heights, even for heavy oil and for thick films. That is why the surface heights are not plotted in the following.

Fig. 4 plots the surface slopes of a particular generated surface, for the same parameters as in Fig. 1. Contrary to the surface heights which show no observable damping, as expected from Fig. 1, a significant damping can be observed. More precisely, as oil damps the higher surface wavenumbers, the higher frequency oscillations of the surface slopes with respect to the horizontal distance are damped. In other words, the oil films act as a low-pass filter. Moreover, with the damping in Fig. 1 being stronger for the third MLB case and weaker for the fourth one (the first and second cases having very similar intermediate dampings), the same observations can be made here in Fig. 4. Even though contaminated surfaces follow the same general slope variations as those of the clean surface, a slight general amplitude damping can be observed, particularly for the stronger damping (heavy oil with $H = 100$ μm). This should have an observable influence on the surface rms slope, as studied in the following.

In Fig. 5, the surface rms slopes of clean and contaminated seas are plotted versus the wind speed u_{10} for low to moderate wind conditions, in the range 2–8 m/s. The oil film is characterized by the same parameters as in Fig. 1. A comparison is also made with the Cox and Munk [34] experimental model, as described in [11]. In [34], the oil film is a mixture consisting of 40% used crankcase oil, 40% diesel oil, and 20% fish oil (with mean oil film thickness on the order of 20 μm [11]). It can be seen that the rms slope of the contaminated (air/oil and oil/sea) interfaces is lower than that of the clean air/sea interface. Once more, as expected, a stronger damping implies a decrease of

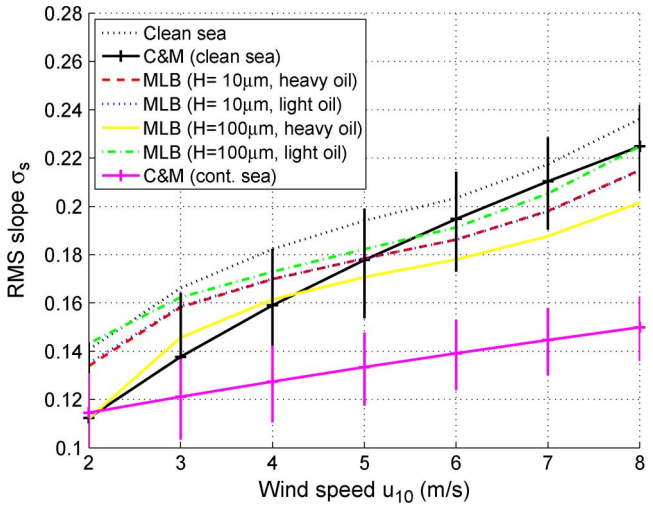

Fig. 5. Surface rms slope σ_s of 1-D clean and contaminated sea surfaces (with the same parameters as in Fig. 1) versus the wind speed u_{10} in the range 2–8 m/s. Comparison with the Cox and Munk experimental model.

the rms slope as the third MLB case is lower than the first and second cases, which, in turn, are lower than the fourth case.

The differences of the contaminated sea with the clean sea are not very much significant compared to the Cox and Munk experimental model [34]. Indeed, the results from the MLB model are significantly higher, especially for the higher wind speeds u_{10} (a better agreement can be found for heavy oil with $H = 500$ μm; see [19, Fig. 5]). A physical explanation of this difference can be given. Indeed, the Cox and Munk experimental results [34] were led for a film which cannot strictly be considered as oil (it has, *a priori*, a different chemical composition and different physical behavior, particularly viscosity). As a consequence, the comparison with the Cox and Munk experimental results is essentially qualitative. Moreover, the results of the MLB with a larger thickness $H = 500$ μm (see [19, Fig. 5]) highlight a good agreement with the Cox and Munk experimental results. Then, this illustrates the coherence of the model.

Thus, owing to a refined hydrodynamic modeling of the surfaces of both clean and contaminated seas, an appropriate electromagnetic modeling can be derived. Beforehand, for the contaminated sea case, both (air/oil and oil/sea) surfaces must be known. In fact, for sea slicks of interest, that is to say for oil film thicknesses up to a few millimeters, the two surfaces can be considered as identical and parallel [35].

In the next section, the influence of rough oil films on rough sea surfaces in the NRCS is calculated and compared with the NRCS of rough clean sea surfaces. Moreover, the TL approach, already used in previous work [11], [19], is tested more thoroughly and is applied with the MLB hydrodynamic model here. Its validity domain is studied for a monostatic configuration by applying it directly to the reference numerical method. The same way is used for the classical approach, which assumes that the electromagnetic wave cannot "see" the oil layer [4], [26]. Finally, a polarimetric analysis is led by means of the polarization ratio, in order to retrieve previous observations led on satellite measurements [12], [18] and to study the influence of various configurations.

III. Electromagnetic Modeling: NRCS of Clean and Contaminated Seas

A. From a Complex Double-Layer Problem to a Single-Layer Problem: TL and Classical Asymptotic Approaches

The problem of electromagnetic wave scattering from a so-called double-layer problem (i.e., made up of a stack of two rough surfaces) is complex to resolve in general. Here, contrary to most electromagnetic asymptotic models which deal with uncorrelated surfaces [36]–[40], the two air/oil and oil/sea interfaces are strongly correlated and can be considered as fully correlated (i.e., identical) for thin oil films up to a few millimeters [35]. As a consequence, the two interfaces of the oil film can be considered as identical and parallel for film thicknesses up to a few millimeters.

Starting from this assumption of the oil film structure, two asymptotic approaches can be derived for simplifying the double-layer electromagnetic problem. First, as led in previous work from the Marangoni effect [11] or for optical applications [19], a so-called TL approach can be applied. It is based on the fact that, because we deal with two identical parallel surfaces for which the capillary waves are strongly damped, the surfaces may be assumed to be locally flat as a first approximation so that the system can be locally seen as a Fabry–Pérot interferometer, as illustrated in [19, Fig. 6]. Indeed, for thin oil films, the locally flat surfaces can be assumed to be parallel. Thus, this double-layer complex problem reduces to a much more simple single-layer problem. Because this assumption is based on the Kirchhoff-tangent plane approximation (KA), it is expected to be valid for regions around the specular direction, corresponding to a monostatic configuration to small incidence angles. Then, we expect this to be valid (at least) where the GO approximation is valid, typically for incidence angles $\theta_i \lesssim 20^\circ$ (indeed, the GO is a further approximation of the KA).

This means that, under this assumption and under the GO, the two-surface problem of NCRS computation can be reduced to a single interface problem (here, the air/oil interface) by using the relation

$$\sigma^{\mathrm{cont,TL}} = \left| \frac{r_{\mathrm{eq}}(\chi_i)}{r_{12}(\chi_i)} \right|^2 \sigma^{\mathrm{air/oil}} \tag{2}$$

with r_{12} as the Fresnel reflection coefficient at the air/oil interface and r_{eq} as the equivalent Fresnel reflection coefficient of the air/oil/sea locally flat layer given by [11, eq. (9)]. χ_i is the local incidence angle, which is related to the incidence and scattering angles θ_i and θ_s, respectively, by the relation $\chi_i = -(\theta_s - \theta_i)/2$. σ^{cont} and $\sigma^{\mathrm{air/oil}}$ are the NRCS of the contaminated sea and of the air/oil interface, respectively. Note that, to be specific, (2) is valid under the Kirchhoff-tangent plane approximation together with the method of stationary phase (KA+MSP), which is valid for very rough surfaces; KA+MSP reduces to the GO for even rougher surfaces.

The second asymptotic approach takes a different point of view. This is the common approach that is used in dealing with modeling of radar backscattering from thin oil slicks [4], [26]; that is why it is called "classical" here. It is based on the fact that, at radar frequencies, the oil film thickness is significantly lower than the electromagnetic wavelength and also that the refractive index of oil is close to 1 and much less than that of sea. Then, the electromagnetic wave does not see the oil film: The air/oil/sea double-layer problem can be assimilated to a simple air/sea problem; the only difference with the clean sea case is that the surface is damped, as described by the MLB. Then, by noting $\sigma^{\mathrm{cont,cl.}}$ as the NRCS of the classical approach, it is expressed as

$$\sigma^{\mathrm{cont,cl.}} = \sigma^{\mathrm{damped\ air/sea}} \tag{3}$$

with $\sigma^{\mathrm{damped\ air/sea}}$ as the NRCS of the damped surfaces described by the MLB (like $\sigma^{\mathrm{air/oil}}$) but by assuming that the lower medium of the surface is the sea. It is interesting to note that Franceschetti *et al.* [26] justified this approach by studying the equivalent Fresnel reflection coefficient r^{eq} of the double-layer structure in comparison with that of the air/sea interface r^{sea}: They showed that, for thin oil films, r^{eq} takes, in general, values close to the ones of r^{sea}.

Then, the "classical" approach may be seen as a further approximation of the TL approach, at least when the Kirchhoff-tangent plane approximation (KA) is valid. In [26], it can be seen that it is valid at a radar frequency $f = 5.6$ GHz for thicknesses $H \leq 2$ mm and for moderate (local) incidence angles χ_i. Nevertheless, this approximation is less good for thicknesses $H > 2$ mm (see [26, Fig. 4] or Fig. 6) or in V (vertical) polarization for local incidence angles χ_i close to the Brewster angle (see [26, Fig. 5] or Fig. 6). This remark also holds at $f = 3$ GHz for thicker films (see [11, Fig. 8] for $H = 10$ mm). Thus, in the X band, the restriction on the thickness is $H \lesssim 1$ mm for the condition to be valid (see Fig. 7 for $f = 10$ GHz). Let us note that in V polarization and for local incidence angles χ_i close to the Brewster angle (on the order of 83° here), the constraint is much harder: on the order of $H \lesssim 0.2$ mm. However, such values of χ_i are not reached in monostatic configurations.

Thus, the TL approach is expected to be valid for monostatic configurations for incidence angles $\theta_i \lesssim 20^\circ$, where the GO is assumed to be valid. To be more specific, the damping of the capillary waves by the oil film should extend this limit to slightly higher values, typically $\theta_i \lesssim 25^\circ$. This limit should increase as the damping increases, that is particularly when the oil viscosity increases and also when the thickness increases (within the validity domain of the Fabry–Pérot assumption). Within this region of validity of the TL approach, the "classical" approach should also be valid for thicknesses $H \lesssim 4$ mm in the C band and $H \lesssim 2$ mm in the X band. Beyond the validity domain of the TL approach, the validity of the "classical" approach is hard to evaluate: It is analyzed hereafter.

In the following section, once the refined MLB hydrodynamic damping model is implemented, the validity domain of both asymptotic electromagnetic approaches is studied more thoroughly by applying them directly to the numerical reference method. That is to say, with the reference numerical method, calculating the NRCS of only the air/oil interface $\sigma^{\mathrm{air/oil}}$, applying (2), and comparing this result directly to the NRCS of the contaminated sea σ^{cont}. This has the advantage of comparing methods of the same kind, contrary to [11] in which the TL approach was applied on the GO and compared to a reference numerical method.

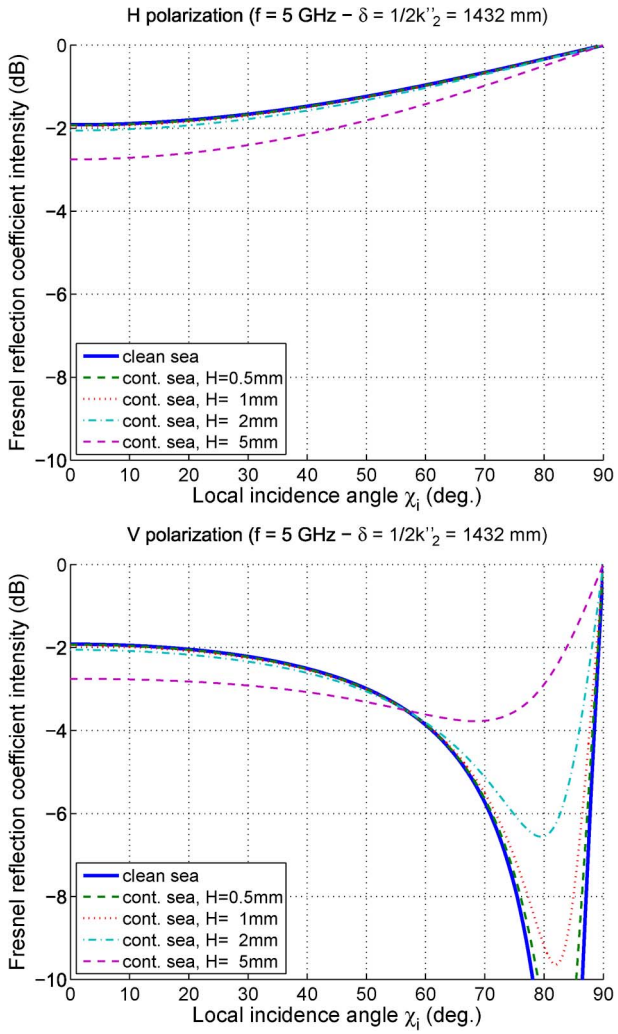

Fig. 6. Intensity of Fresnel reflection coefficients $|r|^2$ (in decibels) of clean and contaminated seas with respect to the local incidence angle χ_i (in degrees) at a radar frequency $f = 5$ GHz for both horizontal (upper figure) and vertical (lower figure) polarizations. For the contaminated sea, several oil film thicknesses are considered: $H = \{0.5; 1; 2; 5\}$ mm. δ represents the penetration depth, defined as $1/(2k_2'')$, with k_2'' as the imaginary part of the wavenumber inside the oil film.

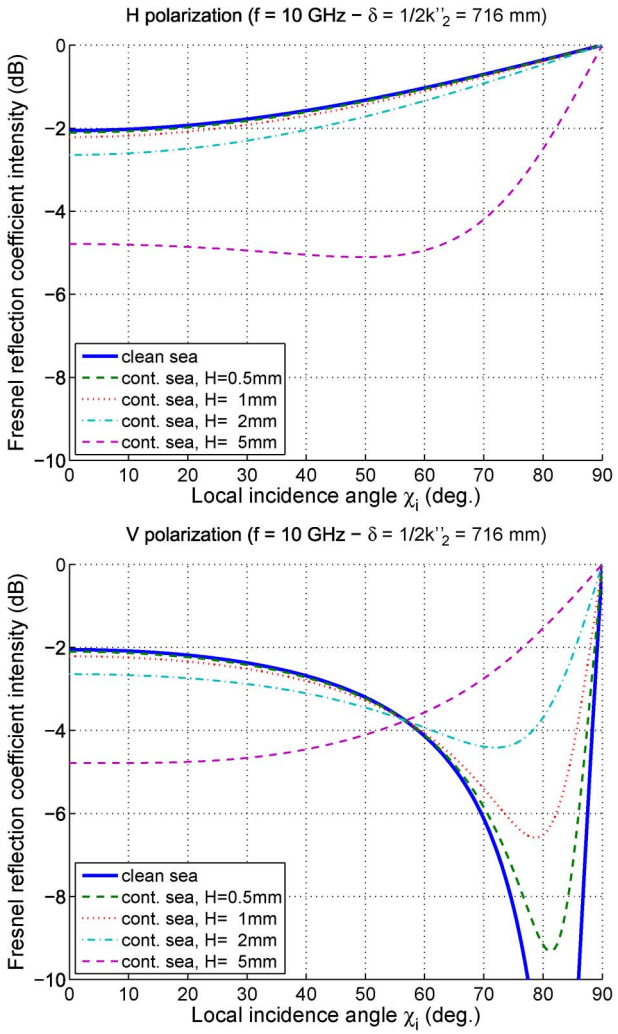

Fig. 7. Simulations for the same parameters as in Fig. 6, except for the radar frequency $f = 10$ GHz.

B. Validity Domain Study of the Two Asymptotic Approaches

This validity domain study is led for 2-D problems only as the actual computer resources make it impossible to resolve the problem of radar scattering from two sea-like surfaces for 3-D problems with "exact" numerical methods. Even for a single sea-like surface, this remains a challenging topic. In spite of this limitation, we know by experience that the results for 2-D problems are very similar to the copolarized (VV and HH) results for 3-D problems. Thus, starting from the following refined 2-D study, chosen asymptotic approaches may be applied to an appropriate analytical model for 3-D problems.

First, let us study a first set of four scenarios, with the following common physical parameters: The oil film is a light oil with kinematic viscosity $\nu_{\text{oil}} = 0.1$ cm^2/s and film thickness $H = 5$ mm. The four scenarios study the distinct influence of the polarization (V or H), the wind speed u_{10} (4 or 7 m/s), and the frequency f (5 or 10 GHz) as follows:

1) $f = 5$ GHz, $u_{10} = 4$ m/s, and V polarization;
2) $f = 5$ GHz, $u_{10} = 4$ m/s, and H polarization;
3) $f = 5$ GHz, $u_{10} = 7$ m/s, and V polarization;
4) $f = 10$ GHz, $u_{10} = 4$ m/s, and V polarization.

For the numerical simulations to follow, the relative permittivities of sea and oil are taken as $\epsilon_{r,\text{sea}} = 69.2 + 35.7i$ and $\epsilon_{r,\text{oil}} = 2.25 + 0.01i$ for $f = 5$ GHz, respectively, and $\epsilon_{r,\text{sea}} = 53.2 + 37.8i$ and $\epsilon_{r,\text{oil}} = 2.25 + 0.01i$ for $f = 10$ GHz. The simulations were led with a numerical reference method based on the method of moments, with the help of acceleration algorithms: the forward–backward (FB) method [41] with spectral acceleration (SA) [42]. Moreover, for the contaminated sea, note that the employed rigorous numerical method is the propagation inside layer expansion (PILE) method [43], [44]. This method makes it possible to rigorously calculate the scattering of electromagnetic waves from stacks of two rough surfaces; one of its advantages is its ability to decompose the total scattered field into its components resulting from the multiple interactions between the two interfaces of the layer. The order of the PILE method p_{PILE}, which corresponds to the number of interactions inside the layer, is then a simulation parameter to be chosen judiciously in order to correctly model the scattering process. Here, in all of the following simulations,

TABLE I
PARAMETERS OF THE PILE+FB-SA METHOD USED FOR THE TWO SCENARIOS DESCRIBED PREVIOUSLY, WITH L_c AS THE SURFACE CORRELATION LENGTH

Scenario #	p_{FB1}	p_{FB2}	x_{d1}/L_c	x_{d2}/L_c	x_{d12}/L_c
1	5	2	0.3	0.06	-
2	5	2	0.3	0.06	-
3	5	2	0.2	0.04	2
4	5	2	0.2	0.04	-

numerical tests showed that $p_{\mathrm{PILE}} = 4$ is a sufficient number. Moreover, only rather significant film thicknesses ($H = 5$ mm) were considered here because the numerical method cannot deal with thicknesses lower than the surface sampling step. Then, the following scenarios are more typical of accidental oil spills than illegal oil spill discharges.

By construction, this method uses the rigorous numerical calculation of the scattering from each surface. Consequently, it is possible to use the single interface acceleration algorithms quoted previously: FB method [41] with SA [42] is then used for each surface, which greatly reduces the computing time and the memory space of the calculation. For each interface and each acceleration algorithm, a parameter must be tuned: For the FB, it is the order of FB, denoted as p_{FB1} and p_{FB2} for the upper and lower surfaces, respectively, and for the SA, it is the distance of strong interactions, denoted as x_{d1} and x_{d2}, respectively. Finally, the computation of the interaction between the two interfaces is also accelerated by the SA, whose tuning parameter is x_{d12}. Then, Table I gives the used values for the four scenarios (note that, for scenarios 1, 2, and 4, the SA is not applied for the coupling calculation because it does not converge). The other simulation parameters are the following: The sampling step $\Delta x = \lambda/10$, the surface length $L = 1.68u_{10}^2$, and the incident beam is a Thorsos wave with tapering parameter $g = L/6$; a Monte Carlo average over 20 surface realizations was performed to obtain the NRCS.

Fig. 8 shows the monostatic NRCS σ (upper figure) of a clean sea computed rigorously with the numerical reference method and of a contaminated sea computed with the numerical reference method either rigorously or by applying the TL or the "classical" approximation. The contaminated sea for a heavy oil (viscosity $\nu_{\mathrm{oil}} = 0.5$ cm^2/s) with the rigorous method is also plotted for comparison. The lower figure shows, for a contaminated sea, the ratio between the NRCS σ of the simplifying approaches and of the rigorous method σ^{rig} for both light and heavy oils. First, it can be seen that, for small observation angles ($\theta_s < 25°$), the contrast between clean and contaminated seas is weak, making the oil slick hardly detectable for this typical configuration and from this sole measurement. Beyond 25°, this contrast increases quickly as θ_s increases, making the oil slick detection possible and easier and easier. The same general remarks hold for the heavy oil, for which the limit of detection occurs earlier (around 20°) and for which the contrast increases more quickly. This is not surprising as a heavier oil induces a stronger damping of the capillary waves and, consequently, a stronger contrast.

Moreover, about the contaminated sea with light oil, the comparison of the rigorous method with the two simplifying approaches highlights a general good agreement (below 2-dB

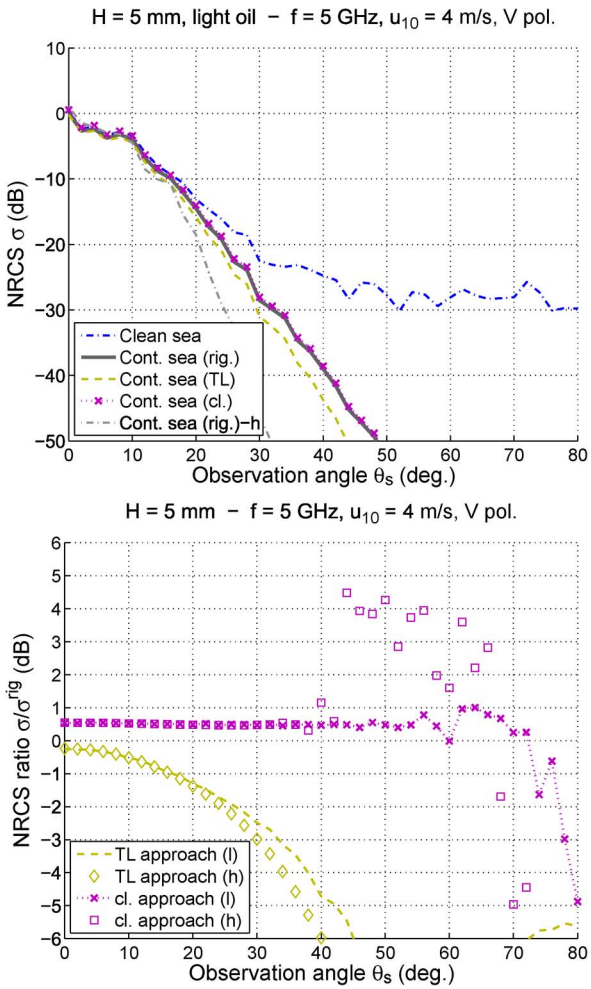

Fig. 8. Monostatic NRCS σ (upper figure) with respect to the observation angle θ_s (in degrees) according to scenario 1, for a light oil with thickness $H = 5$ mm. Comparison between clean and contaminated seas with the rigorous method and with a contaminated sea by using the two simplifying approaches. The contaminated sea for a heavy oil with the rigorous method is also plotted for comparison. The lower figure shows, for a contaminated sea, the ratio between the NRCS of the simplifying approaches and of the rigorous method for both light and heavy oils.

error) up to $\theta_s = 25°$ for the TL approach and at least up to $\theta_s = 72°$ for the classical approach. For small θ_s, the TL approach gives the best agreement, but this approach gradually underestimates the NRCS for increasing θ_s. The classical approach has the great advantage of showing a very good agreement (below 1-dB error) up to at least 72°, with a nearly constant error within this whole angular range. Indeed, beyond 72°, the values of the NRCS are so low that the ratio plot is not reliable. For the heavy oil, similar observations can be made. Here, the classical approach shows a very good agreement (below 1-dB error) up to at least 45°. Thus, the behavior of the TL approach confirms the former qualitative predictions: excellent agreement at 0° and degradation with increasing θ_s.

Fig. 9 plots the numerical results for same simulation parameters as in Fig. 8, except for the H polarization. The same general observations as that for the V polarization can be made here on the NRCS: The general trends are very similar, with increasingly lower NRCS for increasing θ_s. This decrease is weak for the contaminated sea and significant for the clean sea. Then, the limit of detection of the oil slick remains around

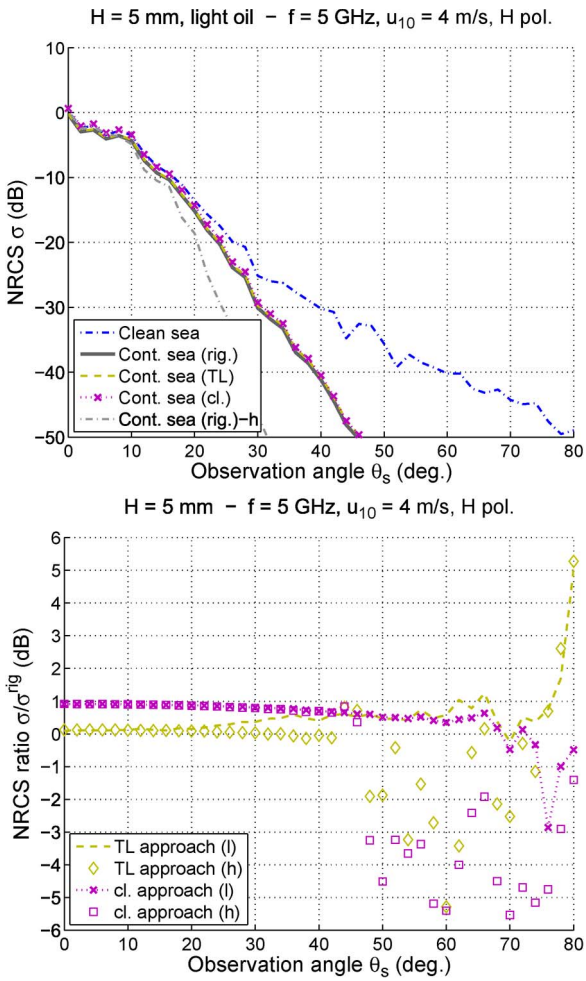

Fig. 9. Same simulation parameters as in Fig. 8, except for the H polarization.

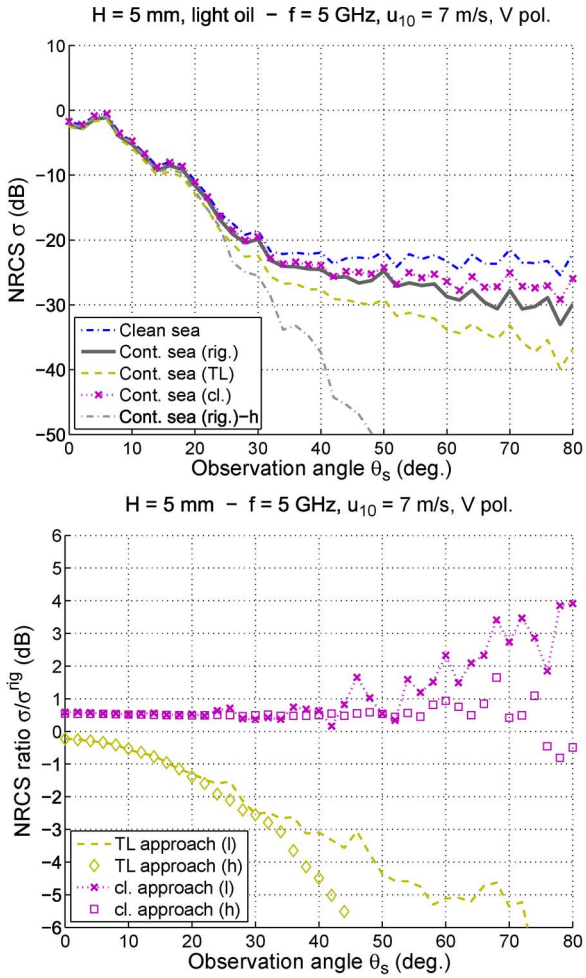

Fig. 10. Same simulation parameters as in Fig. 8, except for the wind speed: $u_{10} = 7$ m/s here.

25°, but the contrast increases less rapidly when θ_s increases. The comparison of the TL and classical approaches with the rigorous method in the lower subfigure shows similar trends for the classical approach and a significantly better general agreement for the TL approach. Indeed, the TL approach shows an excellent agreement (within around 1-dB error) at least up to 42° for heavy oil and 75° for light oil. Note the better agreement for the heavy oil in the range 20–42°, which is consistent with the aforementioned predictions, because a heavier oil induces more capillary wave damping. Like in V polarization, the classical approach shows a very good agreement (1-dB error at the most) with the rigorous method, with nearly constant error, at least up to 45° and 70° for heavy and light oils, respectively.

Fig. 10 plots the numerical results for the same simulation parameters as in Fig. 8, except for the wind speed: $u_{10} = 7$ m/s here. Comparatively to $u_{10} = 4$ m/s, the NRCS levels are mainly increased for moderate θ_s and, in particular, for the contaminated sea. Then, the oil slick is detectable from only 35° for light oil and 25° for heavy oil (with a 3-dB limit of detection), which is in qualitative agreement with measurement observations [21]. This may be attributed to the fact that increasing the wind speed increases the contribution of the gravity waves, which are not damped by the oil film. Also, comparing the slope spectra with wind speeds $u_{10} = 4$ m/s and $u_{10} = 7$ m/s in Figs. 1 and 3, respectively, the contrast between clean and contaminated seas occurs for higher surface wavenumbers for higher wind speeds, inducing a higher Bragg wavenumber at which differences are sensitive. Compared to Fig. 8, similar observations can be made for small observation angles θ_s. The main differences are the following: The TL approach underestimation increases more slowly, and the classical approach is constant only up to 45° for light oil (55° for heavy oil); then, it is valid up to only around 60° for light oil (for heavy oil, it is always within the 2-dB error limit). Both observations may be attributed to the increased contribution of the gravity waves for moderate θ_s.

Fig. 11 plots the numerical results for the same simulation parameters as in Fig. 8, except for the frequency: $f = 10$ GHz here. Note that the heavy oil was computed up to 40° only. Comparatively to $f = 5$ GHz, the main difference comes from the general shape of the contaminated sea compared to the clean sea: It takes lower values even at normal incidence ($\theta_s = 0°$), and the increase of the contrast, which starts from 25° for light oil and 20° for heavy oil, is even stronger here when θ_s increases. Then, the oil slick may be detected for all θ_s for accurate enough sensors (on the order of 2-dB accuracy). About the validity of the TL and classical approaches, the TL approach shows similar features, with increased underestimation

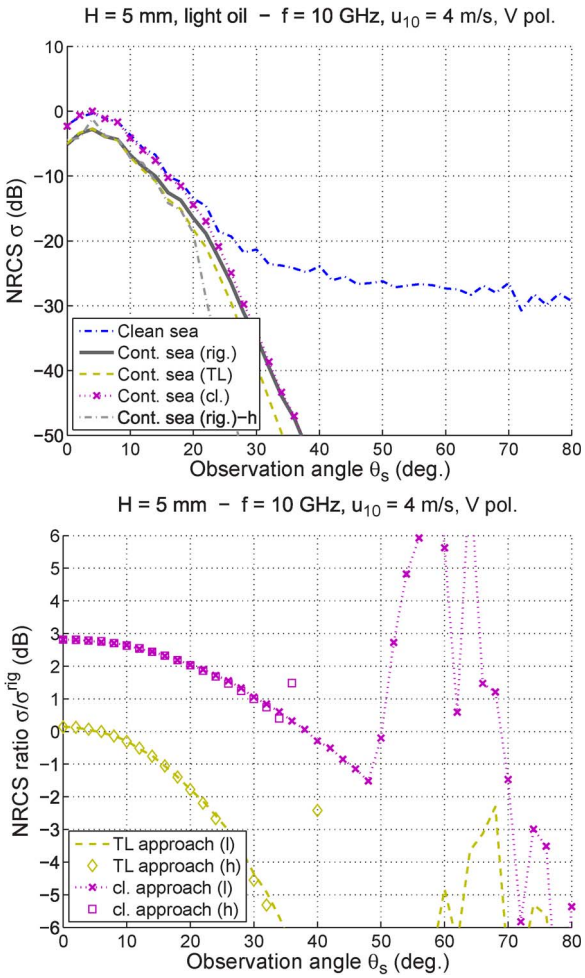

Fig. 11. Same simulation parameters as in Fig. 8, except for the frequency: $f = 10$ GHz here.

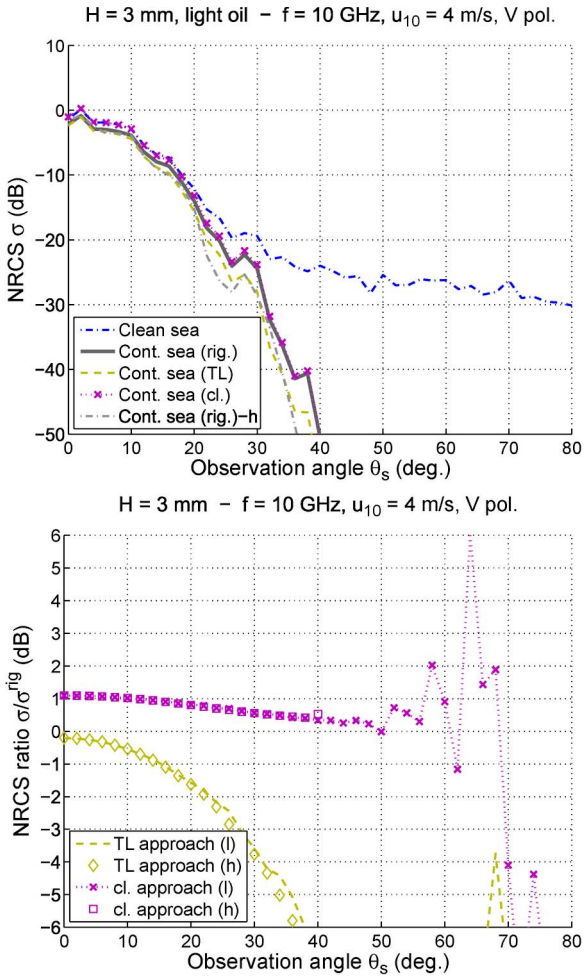

Fig. 12. Same simulation parameters as in Fig. 11 (with $f = 10$ GHz) but with $H = 3$ mm.

for increasing θ_s, so that it is valid up to around 20°. By contrast, the classical approach significantly overestimates the NRCS for low observation angles (up to 3-dB error at 0°). This can be attributed to the fact that here the equivalent Fresnel reflection coefficient of the air/oil/sea double layer is not equivalent to the air/sea Fresnel reflection coefficient any more. This error decreases for increasing θ_s so that it is valid from around 20° and up to at least 35° and 50° for heavy and light oils, respectively. Then, for oil film thicknesses of about $H = 5$ mm, the classical approach seems well adapted for lower frequencies (like that illustrated here in the C band), but it is not the case any more in the X band and, in particular, around nadir. Nevertheless, by keeping a similar thickness-to-wavelength ratio from C band to X band, we expect that the two asymptotic approaches give similar performances. This is illustrated in Fig. 12, where we took $H = 3$ mm (with $f = 10$ GHz). As compared to Fig. 8, indeed, the validity domains of both TL and classical approaches are similar. Moreover, comparing $H = 3$ mm in Fig. 12 to $H = 5$ mm in Fig. 11, as expected, for moderate observation angles ($\theta_s > 20°$), it can be seen that the NRCS decreases when H increases from 3 to 5 mm. This may be attributed to the surface damping by the presence of oil as this damping increases when H increases and because the NRS is sensitive to the surface spectrum in this angular region. By contrast, for small observation angles ($\theta_s < 20°$), only the GO approximation contributes to the scattering process; then, the NRCS is not sensitive to the surface spectrum but only to the surface rms slope whose variations do not have a strong influence from 3 to 5 mm in this angular region (the rms slope varies only slightly in this case). Indeed, as illustrated in Fig. 7 for flat surfaces with $H = \{0.5; 1; 2; 5\}$ mm, the local monostatic NRCS (corresponding to $\chi_i = 0$ in Fig. 7) significantly decreases from 2 to 5 mm: The decrease is about -2.1 dB. Similarly, from 3 mm (not shown here) to 5 mm, the decrease is about -1.4 dB. This mainly explains the differences observed for rough surfaces between Figs. 11 and 12.

These interesting distinct features in the X band deserve plotting another configuration at this frequency. Here, we will change the polarization to H polarization as increasing the wind speed would induce a prohibitive computing time. Then, Fig. 13 plots the same simulation parameters as in Fig. 11 (with $f = 10$ GHz) but for H polarization; only the light oil was considered here. Similar general observations as for $f = 5$ GHz can be made here: From V to H polarization, for moderate θ_s, the contaminated sea is slightly decreased, and the clean sea is strongly decreased. Also, the validity domain of the TL approach is strongly increased, up to nearly 50° here, with perfect agreement up to 30°. The classical approach has the

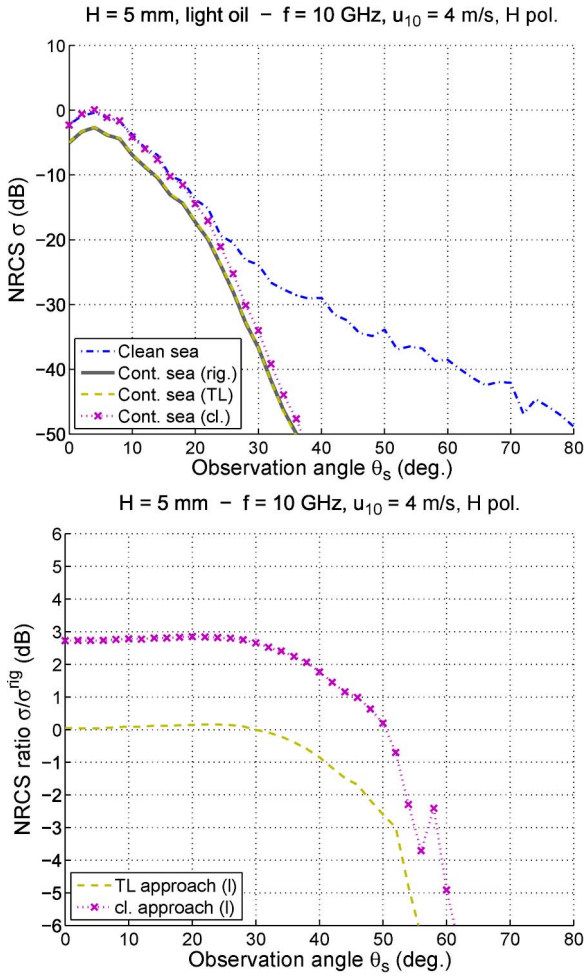

Fig. 13. Same simulation parameters as in Fig. 11 (with $f = 10$ GHz) but for H polarization (light oil only).

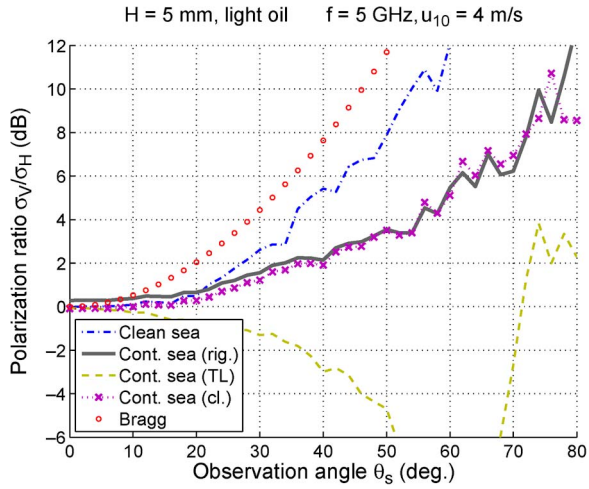

Fig. 14. Polarization ratio σ_V/σ_H (light oil with thickness of 5 mm) for the same simulation parameters as in Fig. 9 (scenarios 1 and 2: $f = 5$ GHz and $u_{10} = 4$ m/s).

same behavior as the TL approach with respect to θ_s and significantly overestimates the NRCS up to 40°. Then, this error decreases, but it strongly increases again from 50° so that it is invalid again from 55°. Thus, for these typical oil film thicknesses, although the classical approach seems very well adapted for lower frequencies (like that illustrated here in the C band), it is not the case in the X band, at least for small observation angles. In what follows, the polarimetric behavior of clean and contaminated seas is analyzed.

C. Polarimetric Behavior

In this section, the polarization behavior of clean and contaminated seas is studied, mainly through the analysis of the (co)polarization ratio σ_V/σ_H; other polarimetric features, like the degree of polarization, the copolarized phase difference, and the copolarization correlation, were also analyzed. They are not plotted here as they did not give significantly new information.

Fig. 14 plots the (co)polarization ratio σ_V/σ_H according to scenarios 1 and 2, with a radar frequency $f = 5$ GHz and a wind speed at 10 m of $u_{10} = 4$ m/s for light oil. The clean sea computed rigorously is compared with the contaminated sea, computed rigorously as well as with both the TL and classical approaches. The polarization ratio predicted by the Bragg theory (or SPM), which is equal to $(1 + 2\tan^2\theta_s)^2$ [45], [46], is also plotted for comparison. Note that the polarization ratio predicted by the GO approximation is practically equal to 1 (0 dB) for all observation angles in monostatic configurations.

For the clean sea, the polarization ratio (PR) starts from 0 dB at zenith $\theta_s = 0$ and is nearly constant up to 15°, which is a characteristic of a GO behavior. This is in agreement with the validity domain of GO for dealing with sea surfaces at these frequencies and wind speeds. Then, the PR slightly increases and then significantly increases from around 30°, with an increase similar to that predicted by Bragg. Then, this is in agreement with the validity domain of SPM for dealing with sea surfaces at these frequencies and wind speeds.

For the contaminated sea, the PR has the same behavior for small θ_s. The main difference is that the increase of the PR is significantly less than that of the clean sea and does not follow the increase predicted by Bragg, at least up to around 70°. This means that, in this region, the Bragg theory (or SPM) alone is not enough to model the scattering mechanism for contaminated seas. The same remark holds for GO in this region. This is an important result as it shows the limits of former analyses of results which were based only on the Bragg theory [6], [25], [33]. Note that this result is coherent with the surface spectrum: looking at Fig. 2, for $f = 5$ GHz and around $\theta_s = 50°$, the Bragg wavenumber given by $k_B = 2k_0 \sin\theta_s$ is equal to around 160 rad/m, around which the curvature spectrum of the contaminated sea is significantly smaller than that of the clean sea. Also, more importantly, this is in agreement with the polarimetric analysis in [12] and [18] which showed that an oil-covered sea surface does not have a pure Bragg-scattering mechanism. Numerical results analyzing the copolarization correlation like that in [12] confirmed this analysis: The correlation is increased for the contaminated sea (not plotted here). This is again logical as the capillary waves are strongly damped when an oil film is at the sea surface. Finally, compared to the "numerically exact" rigorous method, the classical approach correctly predicts the PR, contrary to the TL approach from 10°.

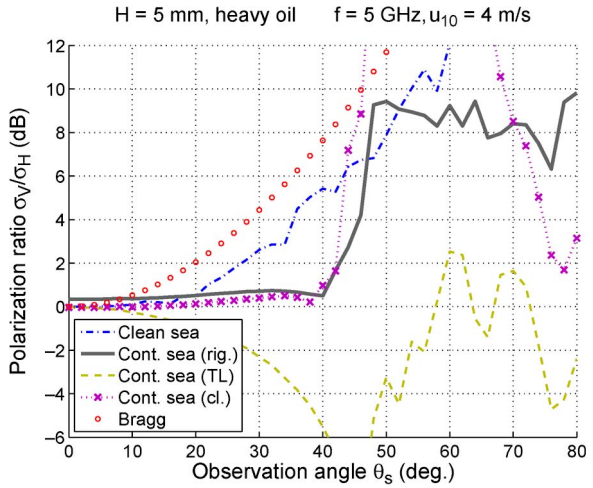

Fig. 15. Same as Fig. 14 but for heavy oil.

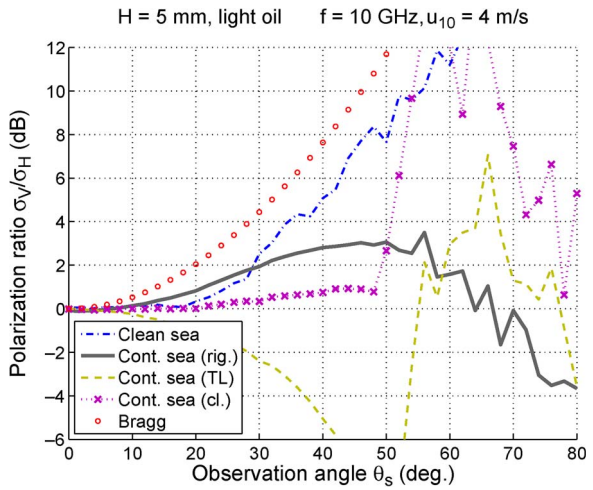

Fig. 16. Polarization ratio σ_V/σ_H (light oil) for the same simulation parameters as in Fig. 11 (scenario 4: $f = 10$ GHz and $u_{10} = 4$ m/s).

Then, Fig. 15 plots the same parameters as in Fig. 14 but for a heavy oil. Comparatively to a light oil, the damping of the capillary waves is much stronger: see Figs. 1 and 2 for $H = 100$ μm, e.g., the contrast between light and heavy oils being even stronger for $H = 5$ mm. As a consequence, the PR of the heavy oil is much closer to 0 for increasing θ_s: It can be seen that the PR is nearly constant and very close to 0 at least up to 40°, which is a characteristic of GO. Note that, above 40°, the strong unphysical increase of the PR is due to the very low NRCS levels, making the results not reliable in this region. Thus, these results show that, at least up to 40°, the scattering mechanism is dominated by GO. Moreover, the classical and TL approaches show the same behaviors as that for the light oil (at least up to 40°). Then, let us have a look at the influence of the frequency on the PR.

Fig. 16 plots the PR of a light oil, for a radar frequency $f = 10$ GHz($u_{10} = 4$ m/s). First, for the clean sea, the PR has a behavior very similar to that for $f = 5$ GHz. The GO validity domain is slightly increased here up to 20°, which is not surprising: As the frequency increases, the Bragg wavenumber increases, making the capillary waves contributive for higher θ_s. For the contaminated sea, the increase of the PR with θ_s is significantly reduced but not down to 0 (note that, once again, the results from 50° are not reliable for the same reason). This means that both the GO and Bragg mechanisms alone are not enough to describe the scattering process in this region, contrary to the clean sea. Moreover, it can be seen here that the classical approach correctly reproduces the PR only in the same region as the TL approach.

Thus, these results are in qualitative agreement with similar analyses made on measurement data [12], [18].

IV. Conclusion

The problem of the hydrodynamic modeling of the surfaces of oil films on the sea is treated by using a physical model, namely the Model of Local Balance (MLB), and the Elfouhaily *et al.* spectrum model for describing the clean sea surface. Then, this physical damping model makes it possible to accurately predict the radar backscattering from clean and contaminated seas. Then, by calculating the NRCS, computations are made from a reference numerical method for 2-D surfaces in order to assess the contrast between clean and contaminated seas for varying configurations, including observation angles θ_s, polarizations (vertical or horizontal), frequencies f, wind speeds u_{10}, thickness H, and characteristics by studying the influence of its viscosity on the NRCS. The main general physical conclusion for moderate observation angles θ_s is as follows: As expected and observed in measurements, the contrast between clean and contaminated sea is increased when the observation angle θ_s increases, the polarization changes from horizontal (H) to vertical (V), the wind speed u_{10} decreases, the frequency f increases, and the oil thickness H or viscosity ν_{oil} increases.

Also, two simplifying approaches in dealing with contaminated seas, called TL and "classical," have been proposed and analyzed. They have the great advantage of reducing the complex double-layer (air/oil and oil/sea) problem to a classical single-layer problem, just like clean seas. Then, their validity domain is studied in detail. It is found, in general, that they have rather complementary validity domains: The TL approach is always valid for small observation angles, which makes it applicable to near nadir sensors like altimeters, whereas the "classical" approach is valid for moderate observation angles, which makes it applicable for satellite applications. A polarimetric analysis is made by focusing on the copolarization ratio. Then, the same qualitative observations as recent work led on satellite measurements (for moderate angles) are found [12], [18], and detailed physical explanations are given. Moreover, this study has the great advantage of being able to study the influence of the different physical parameters: here, the observation angle, the frequency, and the oil viscosity. Thus, these two simplifying approaches make it possible to develop 3-D models of radar backscattering from both clean and contaminated seas by using asymptotic analytical models adapted to sea-like surfaces, like the two-scale model, the small slope approximation, and the weighted curvature approximation [47]. Future work will present such developments and will further validate these models by comparison with measurements.

REFERENCES

[1] M. F. Fingas and C. E. Brown, "Review of oil spill remote sensing," *Spill Sci. Technol. Bull.*, vol. 4, no. 4, pp. 199–208, 1997.

[2] M. Fingas and B. Fieldhouse, "Formation of water-in-oil emulsions and application to oil spill modelling," *J. Hazard. Mater.*, vol. 107, no. 1/2, pp. 37–50, Feb. 2004.

[3] M. Ayari, A. Coatanhay, and A. Khenchaf, "The influence of ripple damping on electromagnetic bistatic scattering by sea surface," in *Proc. Int. Geosci. Remote Sens. Symp.*, Seoul, South Korea, Jul. 2005, pp. 1345–1348.

[4] M. Migliaccio, M. Tranfaglia, and S. Ermakov, "A physical approach for the observation of oil spills in SAR images," *IEEE J. Ocean. Eng.*, vol. 30, no. 3, pp. 496–507, Jul. 2005.

[5] C. Brekke and A. Solberg, "Oil spill detection by satellite remote sensing," *Remote Sens. Environ.*, vol. 95, no. 1, pp. 1–13, Mar. 2005.

[6] M. Gade, Heinrich, Hhnerfuss, and G. M. Korenowski, *Marine Surface Films: Chemical Characteristics, Influence on Air–Sea Interactions and Remote Sensing*. Berlin, Germany: Springer-Verlag, 2006.

[7] S. Derrode and G. Mercier, "Unsupervised multiscale oil slick segmentation from SAR images using a vector HMC model," *Pattern Recognit.*, vol. 40, no. 3, pp. 1135–1147, Mar. 2007.

[8] A. H. S. Solberg, C. Brekke, and P. O. Husoy, "Oil spill detection in RADARSAT and Envisat SAR images," *IEEE Trans. Geosci. Remote Sens.*, vol. 45, no. 3, pp. 746–755, Mar. 2007.

[9] I. Fuks and V. Zavorotny, "Polarization dependence of radar contrast for sea surface oil slicks," in *Proc. IEEE Radar Conf.*, 2007, pp. 503–508.

[10] N. Pinel, C. Bourlier, and J. Saillard, "Forward radar propagation over oil slicks on sea surfaces using the Ament model with shadowing effect," *Progr. Electromagn. Res.*, vol. 76, pp. 95–126, 2007.

[11] N. Pinel, N. Déchamps, and C. Bourlier, "Modeling of the bistatic electromagnetic scattering from sea surfaces covered in oil for microwave applications," *IEEE Trans. Geosci. Remote Sens.*, vol. 46, no. 2, pp. 385–392, Feb. 2008.

[12] F. Nunziata, A. Gambardella, and M. Migliaccio, "On the Mueller scattering matrix for SAR sea oil slick observation," *IEEE Geosci. Remote Sens. Lett.*, vol. 5, no. 4, pp. 691–695, Oct. 2008.

[13] W.-C. Shih and A. B. Andrews, "Modeling of thickness dependent infrared radiance contrast of native and crude oil covered water surfaces," *Opt. Exp.*, vol. 16, no. 14, pp. 10 535–10 542, Jul. 2008.

[14] Y. Lu, Q. Tian, J. Wang, X. Wang, and X. Qi, "Experimental study on spectral responses of offshore oil slick," *Chin. Sci. Bull.*, vol. 53, no. 24, pp. 3937–3941, Dec. 2008.

[15] K. Karantzalos and D. Argialas, "Automatic detection and tracking of oil spills in SAR imagery with level set segmentation," *Int. J. Remote Sens.*, vol. 29, no. 21, pp. 6281–6296, Nov. 2008.

[16] W. Guo and Y. Wang, "A numerical oil spill model based on a hybrid method," *Marine Pollution Bull.*, vol. 58, no. 5, pp. 726–734, May 2009.

[17] M. Migliaccio, F. Nunziata, and A. Gambardella, "On the co-polarized phase difference for oil spill observation," *Int. J. Remote Sens.*, vol. 30, no. 6, pp. 1587–1602, Mar. 2009.

[18] M. Migliaccio, A. Gambardella, F. Nunziata, M. Shimada, and O. Isoguchi, "The PALSAR polarimetric mode for sea oil slick observation," *IEEE Trans. Geosci. Remote Sens.*, vol. 47, no. 12, pp. 4032–4041, Dec. 2009.

[19] N. Pinel, C. Bourlier, and I. Sergievskaya, "Unpolarized emissivity of thin oil films over anisotropic Gaussian seas in infrared window regions," *Appl. Opt.*, vol. 49, no. 11, pp. 2116–2131, Apr. 2010.

[20] D. Jin Kim, W. Moon, and Y.-S. Kim, "Application of TerraSAR-X data for emergent oil-spill monitoring," *IEEE Trans. Geosci. Remote Sens.*, vol. 48, no. 2, pp. 852–863, Feb. 2010.

[21] M. Fingas, *Oil Spill Science and Technology*. Oxford, U.K.: Gulf Professional Publ., 2010.

[22] I. Leifer, W. J. Lehr, D. Simecek-Beatty, E. Bradley, R. Clark, P. Dennison, Y. Hu, S. Matheson, C. E. Jones, B. Holt, M. Reif, D. A. Roberts, J. Svejkovsky, G. Swayze, and J. Wozencraft, "State of the art satellite and airborne marine oil spill remote sensing: Application to the bp deepwater horizon oil spill," *Remote Sens. Environ.*, vol. 124, pp. 185–209, Sep. 2012.

[23] B. Minchew, C. Jones, and B. Holt, "Polarimetric analysis of backscatter from the deepwater horizon oil spill using L-band synthetic aperture radar," *IEEE Trans. Geosci. Remote Sens.*, vol. 50, no. 10, pp. 3812–3830, Oct. 2012.

[24] S. Skrunes, C. Brekke, and T. Eltoft, "Oil spill characterization with multipolarization C- and X-band SAR," in *Proc. IEEE Int. Geosci. Remote Sens. Symp.*, Jul. 2012, pp. 5117–5120.

[25] W. Alpers and H. Hühnerfuss, "Radar signatures of oil films floating on the sea surface and the Marangoni effect," *J. Geophys. Res.*, vol. 93, no. C4, pp. 3642–3648, Apr. 1988.

[26] G. Franceschetti, A. Iodice, D. Riccio, G. Ruello, and R. Siviero, "SAR raw signal simulation of oil slicks in ocean environments," *IEEE Trans. Geosci. Remote Sens.*, vol. 40, no. 9, pp. 1935–1949, Sep. 2002.

[27] K. Lamkaouchi, "Water: A Dielectric Standard. Permittivity of Water–Petrol Mixtures at Microwave Frequencies," Ph.D. dissertation, Bordeaux I Univ., Talence, France, Jun. 1992, in French.

[28] P. Lombardini, B. Fiscella, P. Trivero, C. Cappa, and W. Garrett, "Modulation of the spectra of short gravity waves by sea surface films: Slick detection and characterization with a microwave probe," *J. Atmosp. Ocean. Technol.*, vol. 6, no. 6, pp. 882–890, Dec. 1989.

[29] A. Jenkins and S. Jacobs, "Wave damping by a thin layer of viscous fluid," *Phys. Fluids*, vol. 9, no. 5, pp. 1256–1264, May 1997.

[30] S. Ermakov, S. Salashin, and A. Panchenko, "Film slicks on the sea surface and some mechanisms of their formation," *Dyn. Atmosp. Oceans*, vol. 16, no. 3/4, pp. 279–304, Jan. 1992.

[31] T. Elfouhaily, B. Chapron, K. Katsaros, and D. Vandemark, "A unified directional spectrum for long and short wind-driven waves," *J. Geophys. Res.*, vol. 102, no. C7, pp. 15 781–15 796, Jul. 1997.

[32] W. Plant, "A relationship between wind stress and wave slope," *J. Geophys. Res.*, vol. 87, no. C3, pp. 1961–1967, Mar. 1982.

[33] M. Gade, W. Alpers, H. Hühnerfuss, H. Masuko, and T. Kobayashi, "Imaging of biogenic and anthropogenic ocean surface films by the multifrequency/multipolarization SIR-C/X-SAR," *J. Geophys. Res.*, vol. 103, no. C9, pp. 18 851–18 866, Aug. 1998.

[34] C. Cox and W. Munk, "Measurement of the roughness of the sea surface from photographs of the sun's glitter," *J. Opt. Soc. Amer.*, vol. 44, no. 11, pp. 838–850, Nov. 1954.

[35] E. Kordyban, "Oil thickness variation on wavy water in the presence of wind," *J. Fluids Eng.*, vol. 104, no. 1, pp. 81–87, Mar. 1982.

[36] G. Berginc and C. Bourrely, "The small-slope approximation method applied to a three-dimensional slab with rough boundaries," *Progr. Electromagn. Res.*, vol. 73, pp. 131–211, 2007.

[37] E. Bahar and Y. Zhang, "Diffuse like and cross-polarized fields scattered from irregular layered structures—Full-wave analysis," *IEEE Trans. Antennas Propag.*, vol. 47, no. 5, pp. 941–948, May 1999.

[38] A. Fung, *Microwave Scattering and Emission Models and Their Applications*. Boston, MA, USA: Artech House, 1994.

[39] N. Pinel, J. Johnson, and C. Bourlier, "A geometrical optics model of three dimensional scattering from a rough layer with two rough surfaces," *IEEE Trans. Antennas Propag.*, vol. 58, no. 3, pp. 809–816, Mar. 2010.

[40] M. A. Demir, J. T. Johnson, and T. J. Zajdel, "A study of the fourth-order small perturbation method for scattering from two-layer rough surfaces," *IEEE Trans. Geosci. Remote Sens.*, vol. 50, no. 9, pp. 3374–3382, Sep. 2012.

[41] A. Iodice, "Forward–backward method for scattering from dielectric rough surfaces," *IEEE Trans. Antennas Propag.*, vol. 50, no. 7, pp. 901–911, Jul. 2002.

[42] H.-T. Chou and J. Johnson, "A novel acceleration algorithm for the computation of scattering from rough surfaces with the forward–backward method," *Radio Sci.*, vol. 33, no. 5, pp. 1277–1287, Sep./Oct. 1998.

[43] N. Déchamps, N. de Beaucoudrey, C. Bourlier, and S. Toutain, "Fast numerical method for electromagnetic scattering by rough layered interfaces: Propagation-inside-layer expansion method," *J. Opt. Soc. Amer. A*, vol. 23, no. 2, pp. 359–369, Feb. 2006.

[44] G. Kubické, C. Bourlier, and J. Saillard, "Scattering by an object above a randomly rough surface from a fast numerical method: Extended PILE method combined with FB-SA," *Waves Random Complex Media*, vol. 18, no. 3, pp. 495–519, Aug. 2008.

[45] J. Horstmann, W. Koch, S. Lehner, and R. Tonboe, "Wind retrieval over the ocean using synthetic aperture radar with C-band HH polarization," *IEEE Trans. Geosci. Remote Sens.*, vol. 38, no. 5, pp. 2122–2131, Sep. 2000.

[46] A. Mouche, D. Hauser, J.-F. Daloze, and C.-A. Guérin, "Dual-polarization measurements at C-band over the ocean: Results from airborne radar observations and comparison with Envisat ASAR data," *IEEE Trans. Geosci. Remote Sens.*, vol. 43, no. 4, pp. 753–769, Apr. 2005.

[47] T. Elfouhaily and C.-A. Guérin, "A critical survey of approximate scattering wave theories from random rough surfaces," *Waves Random Media*, vol. 14, no. 4, pp. R1–R40, Oct. 2004.

Nicolas Pinel (M'12) was born in Saint-Brieuc, France, in 1980. He received the Engineering degree and the M.S. degree in electronics and electrical engineering from the Ecole polytechnique de l'université de Nantes (Polytech Nantes), Nantes, France, in 2003 and the Ph.D. degree from the University of Nantes, Nantes, in 2006.

He is currently a Research Engineer with the Institut d'Électronique et de Télécommunications de Rennes (IETR) Laboratory, LUNAM University of Nantes, Nantes. His research interests are in the areas of radar and optical remote sensing, scattering, and propagation. In particular, he works on asymptotic methods of electromagnetic wave scattering from random rough surfaces and layers.

Christophe Bourlier (A'12) was born in La Flèche, France, on July 6, 1971. He received the M.S. degree in electronics from the University of Rennes, Rennes, France, in 1995 and the Ph.D. degree from the Système Électronique et Informatique (SEI) Laboratory, Nantes, France, in 1999.

While at the University of Rennes, he was with the Laboratory of Radiocommunication, where he worked on antenna coupling in the VHF–HF band. He is currently with the Institut d'Électronique et de Télécommunications de Rennes (IETR) Laboratory, LUNAM University of Nantes, Nantes, France. He is also a Researcher with the National Center for Scientific Research, working on electromagnetic wave scattering from rough surfaces and objects for remote sensing applications. He is the author of more than 90 journal articles and conference papers.

Irina Sergievskaya was born in Nizhny Novgorod (Gorky), Russia, on February 11, 1957. She graduated from Gorky State University, Nizhny Novgorod, in 1979 and received the Ph.D. degree from the Institute of Applied Physics, Russian Academy of Sciences, Nizhny Novgorod, in 2004.

Since 1979, she has been with the Institute of Applied Physics, Russian Academy of Sciences, where she is currently the Head of the Laboratory of Optical Methods in Hydrophysics. Her research interests and experience are physics of the sea surface, marine slicks, and their remote sensing. She is the author of more than 43 publications in these fields.